Displacement of Nanofluids in Silica Nanopores: Influenced by Wettability of Nanoparticles and Oil Components

Xiao Wang [1], Senbo Xiao [1], Zhiliang Zhang [1], and Jianying He [1,*]

[1] NTNU Nanomechanical Lab, Department of Structural Engineering, Faculty of Engineering, Norwegian University of Science and Technology (NTNU), 7491 Trondheim, Norway

Corresponding author:
Jianying He
Email: jianying.he@ntnu.no
Tel.: +47-73594686

Abstract

The fundamental understanding of fluids transportation in confined nanopores is essential for groundwater remediation, oil exploration, water purification, etc. Here, all-atom models of various oil components and nanoparticles were put into molecular dynamics simulations for investigating their influences on the displacement of fluid flow into silica nanopore. The simulations indicated that heavy and polar oil components, carrying electronegative atoms (-N, -O), were more favorable to adsorb onto silica nanopore than light and apolar molecules. The polar molecules, such as pyridine, asphaltene, preferred to accumulate at fluids interface, which leaded to increased viscosity of oil phase and hindered spontaneous displacement process. Silica nanoparticles (NPs) in the displacing phase could modulate the fluid-fluid meniscus regardless of hydrophobic or hydrophilic surface modification and slow down the displacement process. Most importantly, the presence of NPs induced pressure difference in the fluids along the nanopore to govern fluids flow process, which shed light on resolving nanoscale water-oil displacement mechanism in sandstone reservoirs. The results provided guidance of designing suitable nanoparticles for targeted applications.

Keywords: Two-phase displacement; Silica nanoparticles; Pressure difference; Molecular dynamics; Enhanced oil recovery (EOR);

1. Introduction

It is known that a large portion of crude oils are still trapped in the pores of reservoir rock after water flooding, and difficult to be explored in petroleum fields by the current technologies [1-3]. Various exploration methods, including chemical injection [4], gas injection [5, 6], had been attempted to enhance oil recovery [7]. The key of state-of-the-art methods is to modify fluid properties, i.e., improving viscosity, reducing interfacial tension, to enhance exploration efficiency for the residual oil in reservoirs. Understanding dynamics of fluids flow in confinement, especially nanopores in stones, is crucial for the design of flooding fluids, given the abundances of nanopores that interconnect large pores and control the permeability of reservoirs. Considering a reservoir with ultra-low permeability, the proportion for nanopores ranging from 0.5 to 100 nm in diameter accounts for 80% of the rock porosity in reservoirs (4500-5600 meter in depth) [8, 9].

Fluids in confined nanopores behave differently from the bulk ones [10, 11]. In hydrophilic confinement, water molecules can form a stable layer near the confining wall, called "immobile water", leading to an increase in fluid viscosity. The viscosity of confined water decreases to bulk value with increased diameter of channel [12]. On the contrary, viscosity for fluids in hydrophobic confinement has an inverse relationship with the diameter, namely water transport enhancement, which is important to water purification[13], CO_2 utilization, etc [14-17]. It is commonly accepted that the properties of confined fluids are influenced by many factors, such as, the addition of chemicals, the wettability and diameters of nanopores [18]. Interestingly, recent experimental results indicated that nanofluids, base fluid containing nanoparticles, have great potential in changing the viscosity of fluids, reducing the water/oil interfacial tension, and altering wettability of rock surface in reservoirs, which can be employed for enhanced oil recovery [19-25].The fundamental understanding of such encouraging results is yet not complete. The atomistic mechanism of nanoparticles for modifying the properties of confined fluids need to be elucidated.

Researches on the fluid flow properties in confined channel have accumulated certain important results, especially the theoretical ones that employed the appropriate Molecular Dynamics (MD) simulations for the nanoscale and complex multi-phase systems [26, 27]. Some of the studies were able to develop and validate models that agree with analytical solution and experimental results [28, 29]. Notably, Wu et.al [18] investigated the flow of water confined in nanopores with different wettability and dimensions by MD simulations. They proposed an accurate model to calculate fluid flux, combining the slip length and viscosity in confined

channel. Other studies utilized MD simulations to capture dynamic microscopic process and revealed interaction and mechanism at nanoscale for various phenomena beyond the range of experimental resolution [30-33]. M. Sedghi et al [34] adopted fully atomistic models to study crude oil/brine displacement in calcite mesopores. They were able to identify the effects of determinants, including temperature, pressure, water salinity and oil composition, on the threshold capillary pressure, and further on controlling flow displacement. C. Chen [35] et al investigated the forced water-oil displacement in capillary by many-body dissipative particle dynamics (MDPD) method. The results showed that water-oil displacement process was closely related with the wettability of water in capillary and miscibility of fluids. Therefore, clarifying the fundamental displacement mechanism of nanofluids under various conditions is very crucial to enhanced oil recovery.

In order to explore the dynamic flow performance and to uncover displacement mechanism of nanofluids for oil recovery in reservoir nanopores, a series of MD simulations with all-atom models were performed here to study the effects of nanoparticles (NPs) with different wettability and oil components on flow behavior in nanopores. Silica, one of the major compositions of glass capillaries and rock minerals in geological environments, was chosen for building the wall of nanopores. Silica NPs were modified by functional groups for varied surface hydrophobicity following relevant applications in oil fields. Adsorption state of crude oil in silica nanopores was first investigated. Nanofluids infiltration into nanopores were then carried out to explore the flow transportation mechanism. Quantitative relationship between displacement length (l) and simulation time (t), interfacial tension and other system properties were analyzed for gaining new insights of the water-oil displacement process in confinement. Moreover, dynamic motion behavior of NPs and pressure difference for fluids along the nanopore were characterized for obtaining the fundamentals of different flow behaviors. The results of this study revealed the micro mechanisms of fluid flow transportation in mineral pores and provided design guidelines for nanoparticles and nanofluids towards enhanced oil recovery (EOR).

2. Model and Simulation Details

2.1 Model systems

2.1.1 Adsorption systems

An all-atom simulation system including a nanopore filled with oil molecules was built for adsorption of crude oil in cylindrical silica nanopores, as shown in Figure 1 (a). The atomistic structure of silica cylindrical nanopore with radius R = ~25 Å was constructed by

removing all atoms around the y-axis center of an amorphous silica block with dimensions of $L_x = L_y = 71.60$ Å and $L_z = 215.18$ Å. The nanopore thus provided sufficient space for the transportation process of nanofluids. Same to former studies [36, 37], the surface of silica nanopore was fully hydroxylated to saturate the bare Si atoms on the internal pore walls, leading to two types of surface functional group configurations: Si-$(OH)_2$ and Si-OH. The silica nanopores were then parameterized by CLAY force filed [38].

Three types of oil components, decane (apolar), pyridine (polar) and asphaltene (polar), were selected as representative apolar and polar molecules of crude oil [6]. Detailed structures of three molecules were shown in Figure 1(b). Three cylindrical oil phase systems, with radius of ~ 20 Å, were built in the silica nanopore: System I pure decane; System II decane (85 wt%) and pyridine (15 wt%); System III decane (87.9 wt%) and asphaltene (12.1 wt%). The mass ratio of polar oil molecules in our systems was close to the range of 11.4 ~ 13.8 wt% [6, 34]. The atomistic parameters from the CHARMM force field were used for all oil molecules [39, 40]. Equilibrium MD simulations of these systems were carried out to obtain steady-state distribution of crude oil in the silica nanopore.

2.1.2 Displacement systems

Simulation systems including nanofluid, oil and the silica nanopore were built to explore the displacement mechanism. Fully equilibrated oil adsorbed systems, with oil molecules stably adsorbing onto silica wall, were selected with the addition of nanofluids. A water-based fluid containing dispersed spherical silica NPs was placed on the end of the silica nanopore, as shown in Figure 1(d). The displacing phase consisted of 20000 water molecules and 16 modified silica NPs. The simple point charge/extend SPC/E model was adopted for water molecules [41]. The same force-field parameters as the nanopore was used for silica NPs. The volume fraction of NPs for two systems were both around 4 %. Because the water phase and nanofluid were highly polar and favorable to the silica pore wall, they were expected to spontaneously migrate into and displace the oil out of the nanopore given sufficient time [42].

The modelling of NPs deserved to be further detailed here. Spherical NPs were first built on α-quartz crystal with the diameter of approximately 13 Å. Unsaturated silicon atoms were removed from surfaces of the NPs and the non-bridging oxygen atoms were saturated with either hydrogen atoms or $–CH_3$ functional groups, thus forming hydrophilic –OH or hydrophobic $–CH_3$ groups, as shown in Figure 1(c). Two types of silica NPs with varied wettability were then used in the study.

2.2 Simulation Details

All the atomistic MD simulations were carried out using the Large atomic/molecular massively parallel simulator (LAMMPS) package [43]. The simulations were conducted in a rectangular periodic box to eliminate the boundary effect [44]. The nanopore fitted periodically to simulation box on X and Z direction, with the cylindrical center axis running along Y direction. Vacuum space was constructed by elongating the simulation box on Y direction, which served as buffer volume for the displaced oil phase out of the nanopore. The short-range nonbonded atom interactions, Lennard-Jones potential with Lorentz-Berthelot mixing rule and electrostatic interactions, were treated with a cutoff distance of 10 Å. The long-range electrostatic interactions were compensated by using the particle-particle-particle-mesh (PPPM) algorithm with a convergence parameter of 10^{-4} [45]. Detailed parameters were given in Table S1 in the Supporting Information.

All the MD simulations were performed under NVT ensemble (constant number of particles, volume, and temperature). The constant temperature was 298 K controlled by Nose-Hoover thermostat with 1.0 ps damping coefficient [46]. Newton's motion equation was integrated by the velocity verlet algorithm. During all the simulations, silica capillary was kept rigid to reduce simulation time except for the modified -OH groups. As all the oil molecules were displaced in 16 ns for NPs-free systems, the same simulation time was applied to all other systems. The simulation results were visualized by the VMD software [47].

3. Results and Discussion

3.1 Adsorption of Crude Oil in Silica Nanopores

Three systems were built to study the adsorption of oil on silica capillary: System I decane; System II decane and pyridine; System III decane and asphaltene. After equilibrium, radial density profiles (RDPs) of three systems were analyzed to characterize the distribution of crude oil molecules in nanopore, as shown in Figure 2. For calculating the RDPs of distinct oil molecule types, the nanopore, ~25 Å in radius, was divided into 25 cylindrical shell in equal thickness. The RDPs of oil types in each system were then obtained by calculating the density of oil molecules inside each shell in equilibrated system snapshots.

Figure 2

As shown in Figure 2(a), the RDP for decane in System I indicated a clear accumulation in the vicinity of the pore wall (about 22 Å), forming a layering of decane molecules inside the nanopore. The overall density for decane in the nanopore was about 0.61 g/cm^3. The second peak is relatively weak compared with the density at the center of pore due to the nonpolar property of decane. In comparison, the density of decane molecules near the pore in System II

(about 22 Å) decreased and the density of pyridine molecules showed a large value of about 0.3 g/cm^3. It indicated that pyridine molecules only appeared in the vicinity of the pore wall, forming a monolayer along the internal surface of nanopore in System II. The distribution of pyridine was illustrated in Figure 2(b). Pyridine tends to repel decane molecules and adsorb onto the wall, owing to its polar molecular property. In contrast to the other two oil molecule types, the heavy oil asphaltene molecules distributed evenly in the nanopore in System III. There was no significant structuring in the asphaltene RDPs. The big molecular size of asphaltene could have been restricted by the curvature of the pore wall (confinement effect), which counteracted the polar molecular properties and hindered its accumulation onto the pore wall. It could also be inferred that if the pore size was much larger than the size of asphaltene molecules, an obvious peak may occur in the radial density profile, similar with that of SII-pyridine. The difference in distributions of pyridine and asphaltene indicated that both molecular polarity and size influence oil components to adsorb onto rock surfaces in real oil field.

The RDPs for different atom types revealed molecular orientation of oil components in equilibrium. As an example of atom RDPs for pyridine shown in Figure 2(c), the N atoms were much closer to the pore wall than the C atoms, with density peak values at 23 Å and 21.5 Å from the pore axis center, respectively. Radial pair distribution function (RDF) between C or N atoms in pyridine and hydrogen atoms on the pore wall also showed the same results, as depicted in Figure 2(d). The polar N atoms were significantly closer to pore wall than the apolar C atoms. The same phenomenon was observed in asphaltene molecules (RDP and RDF profiles shown in Figure S1 in Supporting Information). The results demonstrated that atoms with stronger electronegative property, such as -N, -O, etc., preferred to adsorb on the surface, owing to strong electrostatic interactions. That is to say, heavy and polar oil components have high preference in adsorbing onto the wall of silica nanopores, which will lead to different displacement process from the light and apolar oil molecules.

3.2 Water-Oil Displacement in Silica Nanopores

3.2.1 Effect of oil components

Varied oil components altered the water-oil displacement process in silica nanopore, as shown in Figure 3. All the oil phases in three systems were spontaneously displaced by the water phase. The light and apolar oil, decane, in system I was fully excluded out of the nanopore in 16 ns, showing the highest displacement speed in all the systems. In comparison, polar oil components significantly slowed down the displacement process, as shown by the snapshots of System II and III in Figure 3. The existence of the polar oil molecules, even less than 15

wt%, leaded to dramatically increased viscosity of oil phase in hydrophilic nanopore. The distribution of the polar oil molecules further illustrated their effects on the displacement. Initially, pyridine oil molecules distributed evenly along the silica nanopore in System II. With time evolution, the molecules accumulated at fluids interface and strongly interacted with the water phase owing to the polar nitrogen atoms. The pyridine molecules also showed strong affinity to silica pore wall. Some pyridine molecules even managed to stay with the wall in the water phase at the end of displacement process. Asphaltene molecules in System III demonstrated similar phenomenon, which can also be attributed to the polarity of the molecules. During displacement process, the light molecules (decane) were expected be displaced first from silica nanopore, then followed by heavy and polar oil molecules (pyridine and asphaltene). The water-oil displacement results clearly showed that the addition of heavy and polar oil molecules only increased the viscosity of oil phase, but also brought strong interaction with water phase or the silica pore wall. The high viscosity of oil phase further led to slow displacement speed, in agreement with former studies [48].

Figure 3

3.2.2 Effect of NPs on spontaneous displacement in silica nanopore

The addition of NPs changed the properties of the flooding water, resulting in the different displacement process and mechanism in the confined silica nanopore. Here, the hydrophilic and hydrophobic NPs were added into water phase of the system containing pure decane oil molecules, and the resulted displacement process was shown in Figure 4. The addition of NPs, regardless its wettability, slowed down oil displacement. While the oil phase was fully displaced out of the nanopore by water within 16 ns, there were still large portions of oil molecules remained in the nanopore in systems containing NPs. Despite the similar effect of hydrophilic and hydrophobic NPs on the displacement process, the mechanisms seemed to be rather different due to the distribution of NPs. The hydrophobic NPs, with surfaces modified by -CH_3, either clustered in the water phase or directly migrated into the oil phase, leading to the increased viscosity of oil phase. Most interestingly, the hydrophobic NPs can self-assemble at the water-oil interface, which affected the fluids interfacial tension and migrating of meniscus. In contrast, the hydrophilic NPs, with surfaces modified by -OH, stayed in water-phase and moved very close to fluids interface with time evolution, slowing down the displacement process by increasing viscosity of water phase and potentially reducing fluids interfacial tension.

Figure 4

The dynamics of nanofluid migration in capillary was characterized by the relationship between the displacement length (*l*) of displacing phase and the simulation time (*t*). Same to former studies [49], the location where the local water density is 50% of its bulk value was taken as liquid-liquid interface in the nanopore, depicted in Figure S2 in Supporting Information. As shown in Figure 5, all the interface displacement lengths featured a similar pattern of a fast but short rise at the beginning, followed by a steady increase, which was in good agreement with previous studies [48, 49]. The faster displacement speed of the oil phase by pure water was indicated by bigger displacement at any point of the simulation time. Hydrophilic NPs, shows a slightly faster displacement compared with hydrophobic NPs.

Figure 5

3.2.3 Interfacial thickness for fluids interface

The addition of NPs changed the three-phase contact angle and interfacial tension, which were key properties to determine displacement in nanopores. The interfacial thickness, measured the shape of nanofluid meniscus, is an important quantity for characterizing wettability alteration of the pore walls and fluids interface, and further for elucidating nanoscale displacement mechanism by NPs. Here, the interfacial thickness was calculated based on the "90-90" criterion [50], as the distance where the densities for water and oil phases locate at 90% of their bulk value. The dynamics of the interfacial thickness during the displacement of three systems was given in Figure 6.

Figure 6

The interfacial thickness in all three systems demonstrated an initial increase when water or nanofluids began to enter into the nanopore and to contact with oil phase, echoing the initial stage in displacement curves (Figure 5). Afterwards, the interfacial thickness in all systems reached a plateau, indicating a stable migrating meniscus formed at water-oil interface. However, the interfacial thicknesses were significantly different in three systems, namely thickest in the nanofluid containing hydrophobic NPs (surface modified by $–CH_3$), followed by fluids containing hydrophilic NPs (surface modified by -OH), and thinnest in pure water. It is known that thicker fluids interface means higher miscibility of two phases, and lower interfacial tension [50]. Thus, the interfacial tension between pure water and oil was lowered by the addition of NPs, with the hydrophobic NPs being more pronounced than the hydrophilic ones.

3.3 Mechanism of Spontaneous Water-Oil Displacement in Silica Nanopores

3.3.1 Dynamics of nanoparticles

Addition of NPs, either hydrophobic or hydrophilic, led to significant slowing down of the spontaneous displacement in the silica nanopores. During displacement process, NPs mainly exhibited four states, namely dispersed in the water phase, aggregated in water phase, self-assembly at the fluid interface, and dispersed into the oil phase, as shown in Figure 4. These different states of NPs were responsible for displacement phenomenon in the silica nanopore.

Figure 7

Hydrophilic NPs were found to mainly stay in water phase, and modify the viscosity of water phase to slow down the whole displacement process. The hydrophilic NPs strongly interacted with water molecules in their vicinity to increase the viscosity of nanofluid, as shown in Figure 7. The RDF of oxygen atoms in water molecules and oxygen atoms on the surface of NPs indicated that water molecules form a stable structural layer in a distance of ~1.65 Å (Figure 7(a)). As can be seen in Figure 7(b), the NPs form hydrogen bonds with the close layer of bound water molecules and transport together, which led to a decrease in the displacement of water molecules and overall mobility of the whole water phase. According to Einstein relation and previous studies [51], the viscosity of nanofluids is closely related to the diffusion behavior of liquid molecules. Here, the increased fluid viscosity was depicted by the mean square displacement (MSD) of pure water and nanofluids with hydrophilic NPs shown in Figure 7(c). One interesting phenomenon worth noting was that the hydrophilic NPs seemed to prefer transporting close to the wall of the silica nanopore, despite the existence of the ordered water layer on the wall, which led outperforming adsorption to the hydrophilic NPs, as shown in Figure 7(d). This result is sharply different from our previous study where hydrophilic NPs were found to adsorb onto solid surface and altered the wettability of nanopores [48]. It is yet reasonable when considering the much higher hydrophilicity of silica pore in this study, which could also account for more hydrophilic pores in reality. The detailed three-phase contact angle about three fluids were shown in Section S4 (Supporting Information) to illustrate the influence on displacement process. The results indicated there was small difference about contact angle for all fluids during the dynamic equilibrium stage, revealing that the wettability alteration of capillary by nanoparticles was a less important factor for nanofluids transportation in silica nanopore.

Meanwhile, the hydrophilic NPs favored to move toward the fluids interface. Therefore, simulation with longer time about 28 ns were performed to study if the hydrophilic NPs could self-assemble at the fluids interface during the whole displacement process. The results shown in Figure S4 (in the Supporting Information) indicated migration of some hydrophilic NPs

towards the fluids interface, resulting in the reduction of interfacial tension. In order to briefly probe the resistance of fluid interface and oil phase to the hydrophilic NPs, the steered molecular dynamics (SMD) method was adopted to mimic the migration of nanoparticles in the pore from water to the oil phase [52]. The detailed results are shown in Section S6. From Section S6, larger force is needed for NPs in water phase due to strong interaction between hydrophilic NPs and water phase, while smaller force is needed for NP staying and passing through fluids interface.

Hydrophobic NPs that initially dispersed in the water phase self-aggregated into bigger clusters and assembled at fluids interface and orient to the oil phase. The systems with longer time performed on hydrophobic NPs clearly demonstrated the motion behavior for hydrophobic NPs during displacement process. From Figure S4, it can be seen that the hydrophobic NPs left in water phase self-aggregated into a bigger particle with residual oil molecules, and moved together in the nanopore. The rest of the hydrophobic NPs self-assembled at fluids interface, thus modifying properties of fluid phase, namely increased the viscosity of oil phase and reduced interfacial tension.

3.3.2 Local pressure difference in the nanopore

The local pressure difference in the fluid system underlies the interfacial tension and three-phase contact angle. The existence of nanoparticles, either attracting or repelling water molecules, changes the pressure distribution of fluids, and thus modifies the capillary force and viscous force, resulting in different displacement velocity and efficiency. The local pressure difference of fluids along capillary was characterized to explore the effect of NPs on the displacement process, as shown in Figure 8.

Here, the states for displacement process at 8 ns were chosen to study the local pressure difference of three systems. The addition of NPs resulted in large pressure fluctuation in different sections of fluids along the nanopore. For all three types, the nanofluids outside the capillary showed a relative high pressure, providing driving force for spontaneous displacement process. Comparing the pressure profiles for fluids without and with NPs, the value for oil phase was almost identical and had little fluctuation (the position of interface was obtained from displacement curves in Figure 5). To evaluate the spontaneous displacement process induced by pressure, the total pressure difference along the whole nanopore was calculated by the fluids outside the nanopore. The calculated value for NP-free case was roughly 29.75 atm, while the total pressure difference for fluids with hydrophilic NPs was 21.66 atm, and about 14.66 atm for fluids with hydrophobic NPs. The decreased total pressure

difference for fluids with NPs suggested a decrease in the velocities of fluids entering into the nanopore, which had the same tendency with the displacement velocity in Figure 5.

Figure 8

Meanwhile, the capillary number, a key parameter defined as the ratio of viscous force to capillary force [48], is common used to evaluate the oil recovery efficiency. In EOR process, the bigger the capillary number, the more oil molecules can be explored from the reservoir. In our case, the estimated magnitude for capillary number was 10^{-2}, which could lead to no residual oil and non-aqueous displaced phase left in the reservoir by theory. That means the recovery rate in our system was expected to be 100% [48]. Based on above discussion about pressure difference, the addition of two kinds of nanoparticles decreased capillary pressure of fluids, and thus enhanced the capillary number. Meanwhile, the dispersed hydrophilic NPs in water phase increased fluids viscosity, which also facilitated to displace the residual oil from the reservoir.

Based on above discussions, displacement mechanism of nanofluids into silica nanopores was closely linked with the motion behavior of nanoparticles, and pressure difference induced by different types of nanoparticles was responsible for retarded displacement process. These results suggested that the silica nanoparticles modified with hydrophilic or hydrophobic group can be selected to enhance oil recovery, and hydrophilic NPs modified with –OH should have better performance than the hydrophobic one for the silica nanopore.

Apart from oil components and wettability of NPs, there are still many other factors, such as size of nanopores, volume fractions of NPs in displacing fluid, charge of NPs and other properties related with NPs, and surrounding environments (temperature, pH, etc), significantly influencing flow behavior and fluids properties in silica porous media. For example, Farimani et al. [11] investigated the viscosity of fluids in carbon nanotubes with varied diameters by analyzing spatial diffusion. Results indicated that the viscosity of water was enhanced in smaller size of carbon nanotube, and then decreased close to bulk value with large diameter. Also, studies demonstrated that charged nanoparticle suspensions had a significant enhancement of oil removal efficiency from solid surface [53]. Moreover, smaller nanoparticles with a diameter of 7.0 Å were employed in our previous work [48, 49] to study two-phase displacement, which indicated the displacement length l for water and nanofluids in capillary obeyed the similar relationship of $\sqrt{t}$. However, the volume fractions of nanoparticles and hydrodynamic size of NPs influence the displacement efficiency and velocity of fluids in confined channel. Therefore, more realistic systems and fundamental work should be

investigated to get comprehensive understanding about enhanced oil recovery by nanofluids in further studies.

4. Conclusion

All-atom molecular dynamics simulations were employed to study the influence of nanoparticles and oil components on migration of nanofluids into silica nanopore. Two types of nanoparticles and three oil mixtures were selected. The simulations indicated that heavy and polar oil components with the electronegative atoms (-N, -O) favored to adsorb onto silica nanopore, which caused polar oil component accumulating at the fluids interface and the pore wall, and subsequently led to decreased displacement velocities. The addition of nanoparticles modulated the fluid-fluid meniscus and hindered displacement process compared with pure water flooding. Quantitative analysis indicated that the interfacial thicknesses for three kinds of fluids had inverse tendency with displacement length. Hydrophilic NPs well dispersed in water, and resulted in an increase in the viscosity of water phase. According to the analyses on the fluid motion behavior, there was always a water layer between hydrophilic NPs and silica capillary, and high force was needed for hydrophilic NPs to break hydrogen bonds among water molecules and interactions between water layer and silica surface. For hydrophobic NPs, they tended to transport into oil phase, and the residual NPs in water phase aggregated into a bigger cluster, all of which gave rise to the decreased displacement velocity. The addition of NPs altered the local pressure in liquid phase. The calculated total pressure difference for fluids had the same tendency with the decreased displacement velocity. Therefore, the pressure difference induced by nanoparticles were the main driving force for retarded spontaneous water-oil displacement in silica nanopores. The capillary number suggested that the modified silica nanoparticles with –OH NPs may have better performance than hydrophobic –CH3 NPs in applications of oil recovery. Our findings not only revealed the crude oil exploration process in silica based sandstone, but also uncovered the intrinsic spontaneous two-phase displacement mechanism influenced by nanoparticles, which provided a guidance for modifying the displacement rate and designing suitable nanoparticles for practical applications such as EOR.

Supplementary Materials: The following are available online at http://.

Acknowledgments: This work is supported by the Research Council of Norway, Aker BP ASA, and Wintershall Norge AS via WINPA project (NANO2021 and PETROMAKSII

234626). The computational resources are provided by Norwegian Metacenter for Computational Science (NOTUR NN9110k and NN9391k).

Conflicts of Interest: The authors declare no conflict of interest.

References

1. E. A. Taborda, C. A. Franco, M. A. Ruiz, V. Alvarado and F. B. Cortés, Experimental and Theoretical Study of Viscosity Reduction in Heavy Crude Oils by Addition of Nanoparticles, *Energy Fuels*, 2017, **31**, 1329-1338.
2. C. Negin, S. Ali and Q. Xie, Application of nanotechnology for enhancing oil recovery – A review, *Petroleum*, 2016, **2**, 324-333.
3. A. Bera and H. Belhaj, Application of nanotechnology by means of nanoparticles and nanodispersions in oil recovery - A comprehensive review, *J. Nat. Gas. Sci. Eng.*, 2016, **34**, 1284-1309.
4. J. Lee, A. Nikolov and D. Wasan, Effects of Micellar Structuring and Solubilized Oil on the Kinetic Stability of Aqueous Foams, *Ind. Eng. Chem. Res.*, 2014, **53**, 18891-18899.
5. Y. Xiong, C. Wang, J. Jiang and H. Deng, A Simple Method To Calculate the Viscosity of Heavy Oil Saturated with Supercritical CO2Using Correlations, *Energy Fuels*, 2016, **30**, 2805-2812.
6. Y. Yan, C. Li, Z. Dong, T. Fang, B. Sun and J. Zhang, Enhanced oil recovery mechanism of CO2 water-alternating-gas injection in silica nanochannel, *Fuel*, 2017, **190**, 253-259.
7. K. Falk, B. Coasne, R. Pellenq, F. J. Ulm and L. Bocquet, Subcontinuum mass transport of condensed hydrocarbons in nanoporous media, *Nat. Commun.*, 2015, **6**, 6949.
8. J. M. de Almeida and C. R. Miranda, Improved oil recovery in nanopores: NanoIOR, *Sci. Rep.*, 2016, **6**, 28128.
9. T. J. Katsube and M. A. Williamson, Effects of Diagenesis on Shale Nano-pore Structure and Implications for Sealing Capacity, *Clay Minerals*, 1994, **29**, 451-461.
10. L. Wang, M. S. H. Boutilier, P. R. Kidambi, D. Jang, N. G. Hadjiconstantinou and R. Karnik, Fundamental transport mechanisms, fabrication and potential applications of nanoporous atomically thin membranes, *Nat. Nanotechnol.*, 2017, **12**, 509-522.
11. A. B. Farimani and N. R. Aluru, Spatial diffusion of water in carbon nanotubes: from fickian to ballistic motion, *J. Phys. Chem. B*, 2011, **115**, 12145-12149.
12. P. J. Feibelman, Viscosity of Ultrathin Water Films Confined between Aluminol Surfaces of Kaolinite: Ab Initio Simulations, *J. Phys. Chem. C.*, 2013, **117**, 6088-6095.
13. K. Yang, J. Wang, X. Chen, Q. Zhao, A. Ghaffar and B. Chen, Application of graphene-based materials in water purification: from the nanoscale to specific devices, *Environ. Sci.: Nano*, 2018, **5**, 1264-1297.
14. H. G. Park and Y. Jung, Carbon nanofluidics of rapid water transport for energy applications, *Chem. Soc. Rev.*, 2014, **43**, 565-576.
15. M. Heiranian, A. B. Farimani and N. R. Aluru, Water desalination with a single-layer MoS2 nanopore, *Nat. Commun.*, 2015, **6**, 8616.

16. M. Ma, F. Grey, L. Shen, M. Urbakh, S. Wu, J. Z. Liu, Y. Liu and Q. Zheng, Water transport inside carbon nanotubes mediated by phonon-induced oscillating friction, *Nat. Nanotechnol.*, 2015, **10**, 692-695.
17. C. H. Lee, B. Tiwari, D. Zhang and Y. K. Yap, Water purification: oil-water separation by nanotechnology and environmental concerns, *Environ. Sci.: Nano*, 2017, **4**, 514-525.
18. K. Wu, Z. Chen, J. Li, X. Li, J. Xua and X. Dong, Wettability effect on nanoconfined water flow, *Proc. Nat. Acad. Sci. U.S.A.*, 2017, **114**, 3358-3363.
19. B. Wei, Q. Li, F. Jin, H. Li and C. Wang, The Potential of a Novel Nanofluid in Enhancing Oil Recovery, *Energy Fuels*, 2016, **30**, 2882-2891.
20. D. Luo, F. Wang, J. Zhu, F. Cao, Y. Liu, X. Li, R. C. Willson, Z. Yang, C. W. Chu and Z. Ren, Nanofluid of graphene-based amphiphilic Janus nanosheets for tertiary or enhanced oil recovery: High performance at low concentration, *Proc. Nat. Acad. Sci. U.S.A.*, 2016, **113**, 7711-7716.
21. A. D. N. Darsh T. Wasan, Spreading of nanofluids on solids, *Nature*, 2003, **423**, 156-159.
22. J. M. Berlin, J. Yu, W. Lu, E. E. Walsh, L. Zhang, P. Zhang, W. Chen, A. T. Kan, M. S. Wong, M. B. Tomson and J. M. Tour, Engineered nanoparticles for hydrocarbon detection in oil-field rocks, *Energy Environ. Sci.*, 2011, **4**, 505-509.
23. M. D. Becker, Y. Wang, K. D. Pennell and L. M. Abriola, A multi-constituent site blocking model for nanoparticle and stabilizing agent transport in porous media, *Environ. Sci.: Nano*, 2015, **2**, 155-166.
24. H. Zhang, A. Nikolov and D. Wasan, Enhanced Oil Recovery (EOR) Using Nanoparticle Dispersions: Underlying Mechanism and Imbibition Experiments, *Energy Fuels*, 2014, **28**, 3002-3009.
25. N.A. Ogolo, O.A. Olafuyi and M. O. Onyekonwu, presented in part at the SPE Arabia Section Technical Symposium and Exhibition, AI-Khobar, Saudi Arabia, 8-11 April, 2012.
26. D. Schebarchov and S. C. Hendy, Uptake and withdrawal of droplets from carbon nanotubes, *Nanoscale*, 2011, **3**, 134-141.
27. E. Oyarzua, J. H. Walther, A. Mejia and H. A. Zambrano, Early regimes of water capillary flow in slit silica nanochannels, *Phys. Chem. Chem. Phys.*, 2015, **17**, 14731-14739.
28. G. Martic, F. Gentner, D. Seveno, D. Coulon and J. D. Coninck, A Molecular Dynamics Simulation of Capillary Imbibition, *Langmuir*, 2002, **18**, 7971-7976.
29. N. Giovambattista, A. B. Almeida, A. M. Alencar and S. V. Buldyrev, Validation of Capillarity Theory at the Nanometer Scale by Atomistic Computer Simulations of Water Droplets and Bridges in Contact with Hydrophobic and Hydrophilic Surfaces, *J. Phys. Chem. C*, 2016, **120**, 1597-1608.
30. H. Yan and S. Yuan, Molecular Dynamics Simulation of the Oil Detachment Process within Silica Nanopores, *J. Phys. Chem. C.*, 2016, **120**, 2667-2674.

31. H. Wu, J. Chen and H. Liu, Molecular Dynamics Simulations about Adsorption and Displacement of Methane in Carbon Nanochannels, *J. Phys. Chem. C.*, 2015, **119**, 13652-13657.
32. S. Xiao, J. He and Z. Zhang, Nanoscale deicing by molecular dynamics simulation, *Nanoscale*, 2016, **8**, 14625-14632.
33. J. Zhong, M. Kumar, J. S. Francisco and X. C. Zeng, Insight into Chemistry on Cloud/Aerosol Water Surfaces, *Acc. Chem. Res.*, 2018, **51**, 1229-1237.
34. M. Sedghi, M. Piri and L. Goual, Atomistic Molecular Dynamics Simulations of Crude Oil/Brine Displacement in Calcite Mesopores, *Langmuir*, 2016, **32**, 3375-3384.
35. C. Chen, L. Zhuang, X. Li, J. Dong and J. Lu, A many-body dissipative particle dynamics study of forced water-oil displacement in capillary, *Langmuir*, 2012, **28**, 1330-1336.
36. J. Wu, J. He, O. Torsæter and Z. Zhang, presented in part at the SPE International Oilfield Nanotechnology Conference, Noordwijk, The Netherlands, 12-14, June, 2012.
37. K. Yamashita and H. Daiguji, Molecular Dynamics Simulations of Water Uptake into a Silica Nanopore, *J. Phys. Chem. C*, 2015, **119**, 3012-3023.
38. R. T, Cygan, Jian-Jie Liang and A. G. Kalinichev, Molecular Models of Hydroxide, Oxyhydroxide, and Clay Phases and the Development of a General Force Field, *J. Phys. Chem. B*, 2004, **108**, 1255-1266.
39. S. Patel, C. L and B. III, CHARMM Fluctuating Charge Force Field for Proteins: I Parameterization and Application to Bulk Organic Liquid Simulations, *Patel and Brook*, 2003, **25**, 1-15.
40. K. Vanommeslaeghe, E. Hatcher, C. Acharya, S. Kundu, S. Zhong, J. Shim, E. Darian, O. Guvench, P. Lopes, I. Vorobyov and A. D. Mackerell, Jr., CHARMM general force field: A force field for drug-like molecules compatible with the CHARMM all-atom additive biological force fields, *J. Comput. Chem.*, 2010, **31**, 671-690.
41. H. J. C. Berendsen, J. R. Grigera and T. P. Straatsma, The missing term in effective pair potentials, *J. Phys. Chem.*, 1987, **91**, 6269-6271.
42. K. Shirono and H. Daiguji, Molecular Simulation of the Phase Behavior of Water Confined in Silica Nanopores, *J. Phys. Chem. C*, 2007, **111**.
43. S. Plimpton, Fast Parallel Algorithms for Short-Range Molecular Dynamics, *J. Comput. Phys.*, 1995, **117**, 1-19.
44. B. Liu, C. Wang, J. Zhang, S. Xiao, Z. Zhang, Y. Shen, B. Sun and J. He, Displacement Mechanism of Oil in Shale Inorganic Nanopores by Supercritical Carbon Dioxide from Molecular Dynamics Simulations, *Energy Fuels*, 2017, **31**, 738-746.
45. T. Darden, D. York and L. Pedersen, Particle mesh Ewald: An N·log(N) method for Ewald sums in large systems, *J. Chem. Phys.*, 1993, **98**, 10089-10092.
46. S. Nosé, A molecular dynamics method for simulations in the canonical ensemble, *Mol. Phys.*, 1984, **52**, 255-268.

47. W. Humphrey, A. Dalke and K. Schulten, VMD: Visual molecular dynamics, *J. Mol. Graph.*, 1996, **14**, 33-38.
48. X. Wang, Z. Zhang, O. Torsaeter and J. He, Atomistic insights into the nanofluid transport through an ultra-confined capillary, *Phys. Chem. Chem. Phys.*, 2018, **20**, 4831-4839.
49. X. Wang, S. Xiao, Z. Zhang and J. He, Effect of Nanoparticles on Spontaneous Imbibition of Water into Ultraconfined Reservoir Capillary by Molecular Dynamics Simulation, *Energies*, 2017, **10**, 506.
50. SeungSoon Jang, ShiangTai Lin, Prabal K. Maiti, Mario Blanco, W. A. G. III, Patrick Shuler and Y. Tang, Molecular Dynamics Study of a Surfactant-Mediated Decane-Water Interface: Effect of Molecular Architecture of Alkyl Benzene Sulfonate, *J. Phys. Chem. B*, 2004, **108**, 12130-12140.
51. J. A. Thomas and A. J. H. McGaughey, Reassessing Fast Water Transport Through Carbon Nanotubes, *Nano Lett*, 2008, **8**, 2788-2793.
52. S. Park and K. Schulten, Calculating potentials of mean force from steered molecular dynamics simulations, *J. Chem. Phys.*, 2004, **120**, 5946-5961.
53. F.C. Wang and H.A. Wu, Enhanced oil droplet detachment from solid surfaces in charged nanoparticle suspensions, *Soft Matter*, 2013, **9**, 7974.

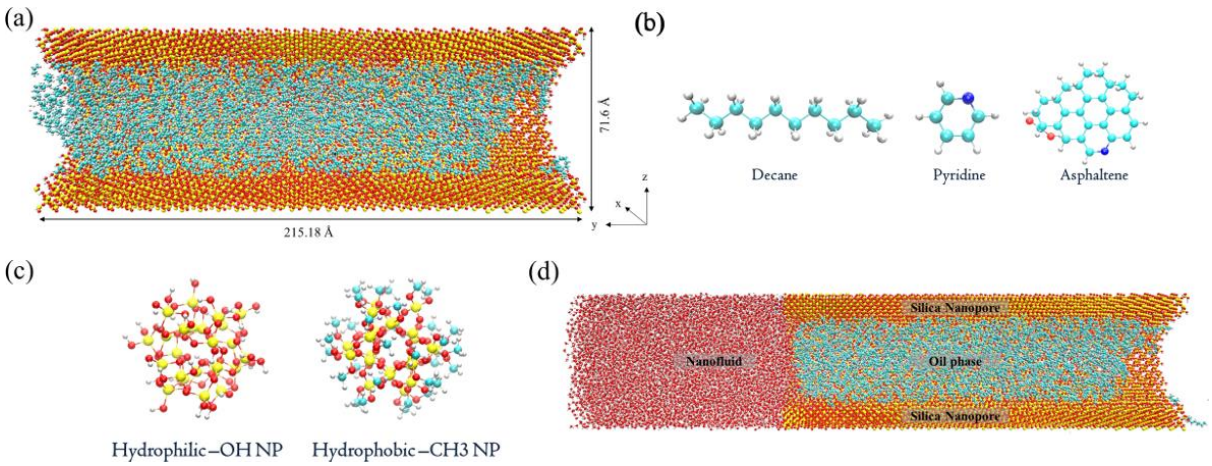

Figure 1 Atomistic models: (a) an example silica nanopore filled with decane molecules; (b) three types of oil components; (c) silica nanoparticles with hydrophilic and hydrophobic surface modifications by –OH and $–CH_3$, respectively; (d) a two-phase displacement system. The colors for different atoms: oxgen (red), hydrogen (white), silicon (yellow), carbon (cyan), and nitrogen (blue).

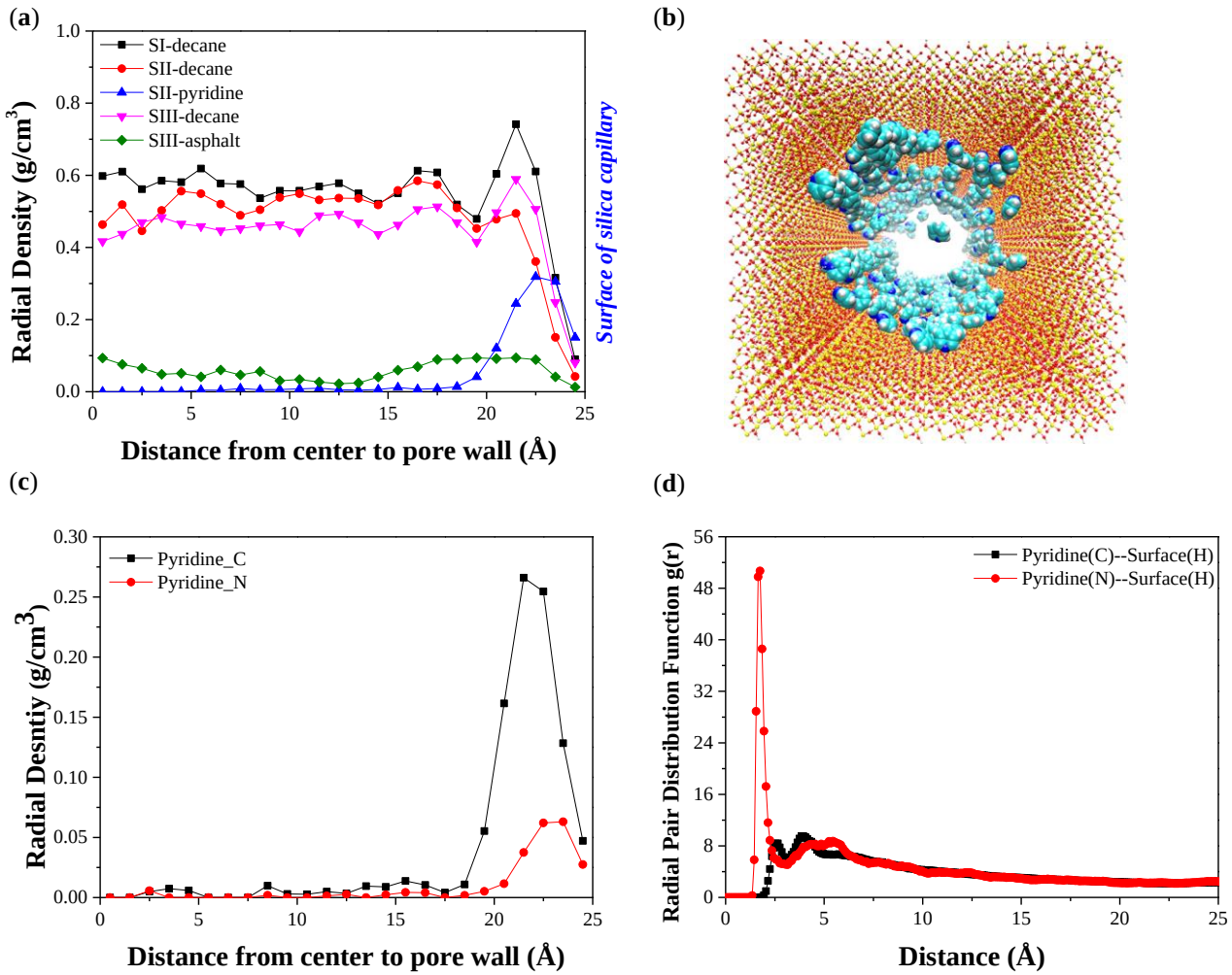

Figure 2 (a) Radial density profiles for decane, pyridine, and asphaltene from center axis to the wall of the silica nanopore; (b) adsorption of pyridine molecules in silica nanopore; (c) radial density profiles for carbon and nitrogen atoms in pyridine molecules; (d) radial pair distribution function between carbon or nitrogen in pyridine and hydrogen in silica surface, respectively.

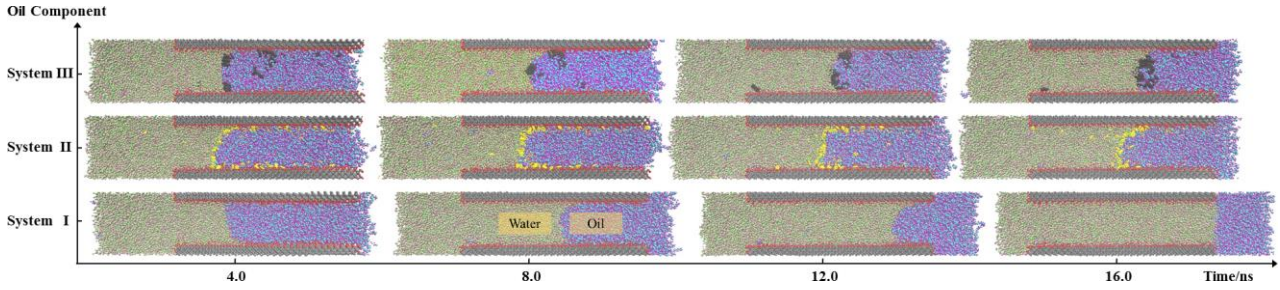

Figure 3 Flow snapshots with different oil molecules by pure water in silica nanopores with time evolution. System I: decane; System II: decane and pyridine; System III: decane and asphaltene. The meaning of colors: nanopore (grey and red), water (green and pink), decane (purple and blue), pyridine (yellow), asphaltene (black).

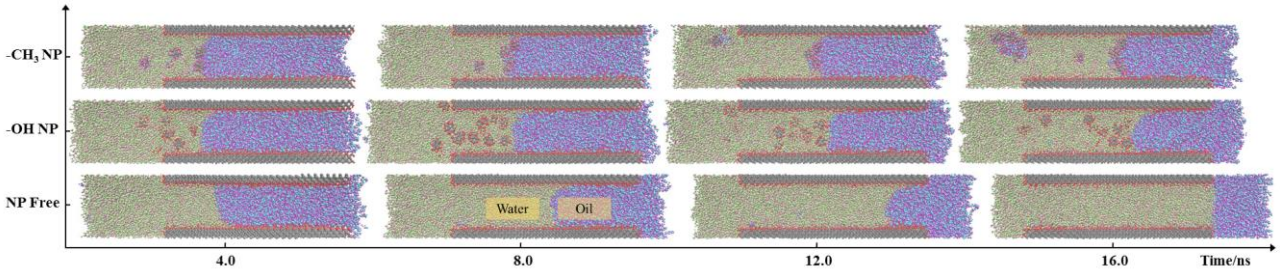

Figure 4 Flow snapshots of pure decane by the nanofluids and pure water (NP Free) in silica nanopores. The meaning of colors: nanopore (grey and red), water (green and pink), decane (purple and blue), hydrophilic -OH NPs (grey and red), hydrophobic -CH_3 NPs (grey and purple).

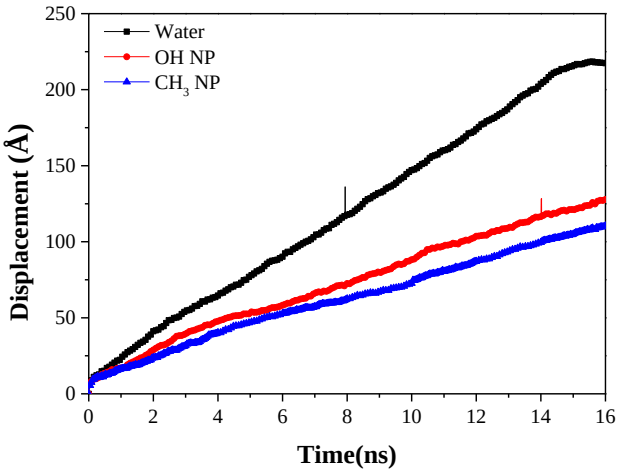

Figure 5 The displacement of nanofluids as a function of time in three systems.

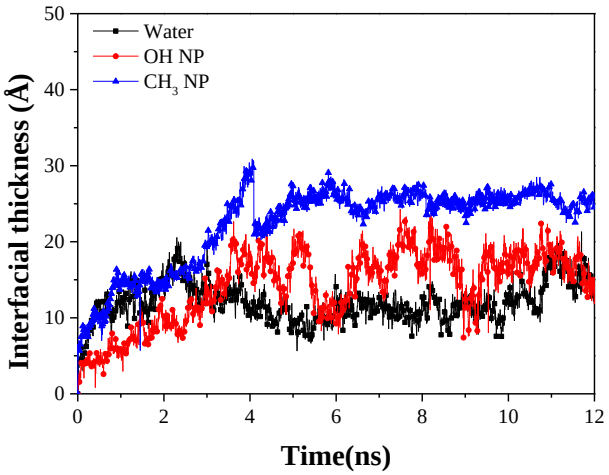

Figure 6 Dynamic interfacial thickness of the fluid interfaces with time evolution.

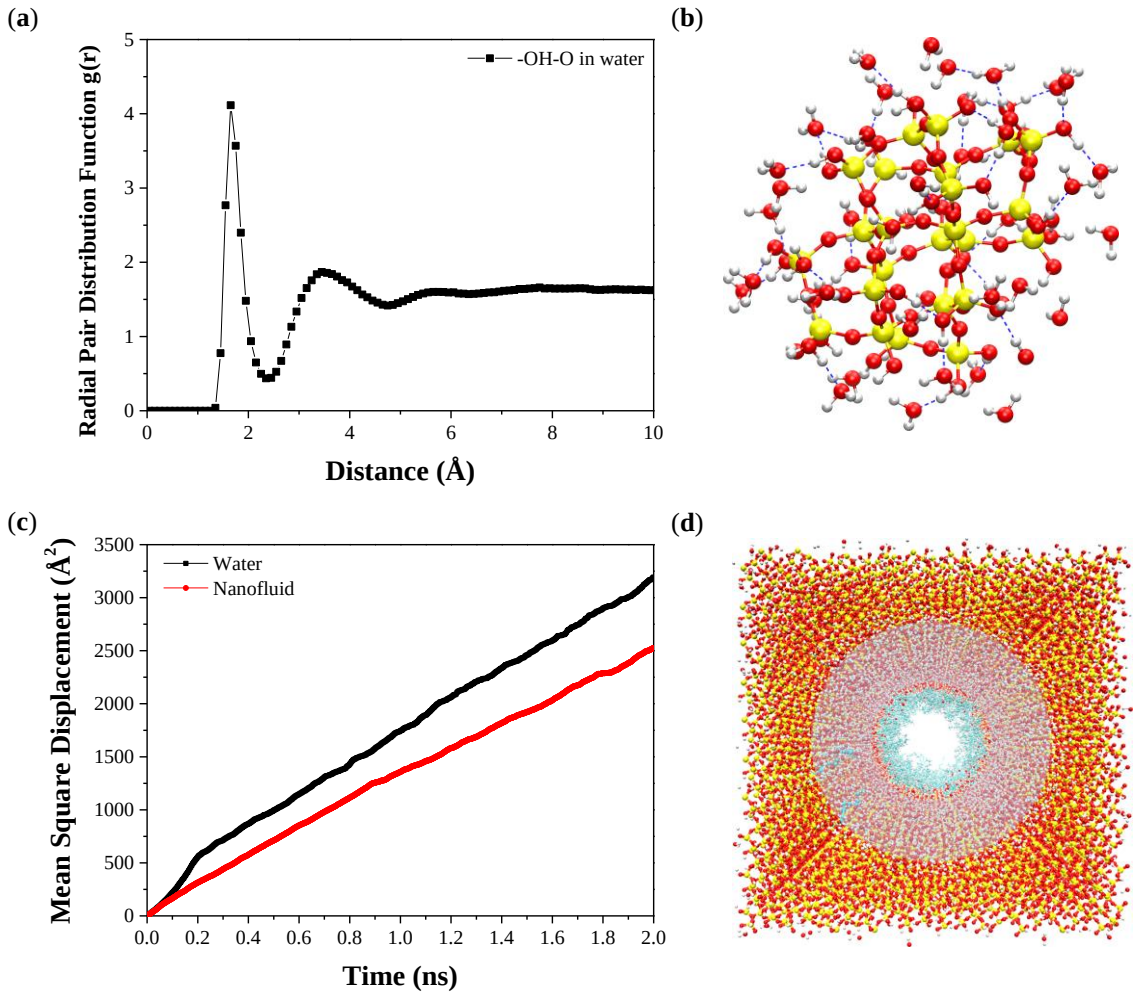

Figure 7 (a) Radial pair distribution function between water oxygen atoms around the hydrophilic NP surface; (b) snapshot of the closest water layer around a hydrophilic NP and hydrogen bonding indicated by grey dash line, atom colors shown in Figure 1; (c) Mean Square Displacement for water molecules in pure water and in nanofluids with hydrophilic NPs in the nanopores; (4) snapshot of the closest water layer to the wall of the nanopore.

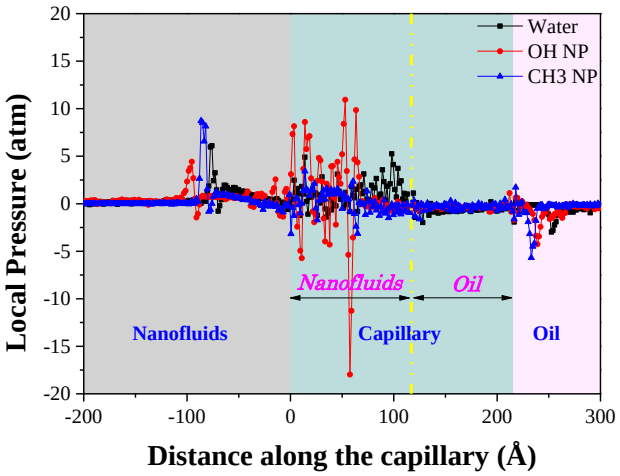

Figure 8 Local pressure distribution in the fluids along the axial direction of the silica nanopore.

Graphic

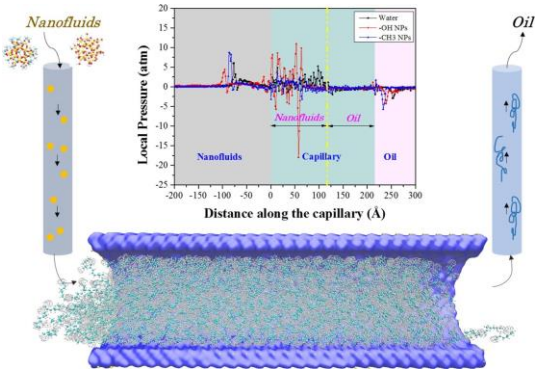
Nanofluids
Oil
Water
-OH NPs
-CH3 NPs
Local Pressure (atm)
Nanofluids
Oil
Nanofluids
Capillary
Oil
Distance along the capillary (Å)